

LETTER TO THE EDITOR

# Possible pair-instability supernovae at solar metallicity from magnetic stellar progenitors

Cyril Georgy<sup>1</sup>, Georges Meynet<sup>1</sup>, Sylvia Ekström<sup>1</sup>, Gregg A. Wade<sup>2</sup>, Véronique Petit<sup>3</sup>, Zsolt Keszthelyi<sup>2,4</sup>, and Raphael Hirschi<sup>5,6</sup>

<sup>1</sup> Geneva Observatory, University of Geneva, Maillettes 51, 1290 Sauverny, Switzerland  
e-mail: cyril.georgy@unige.ch

<sup>2</sup> Department of Physics, Royal Military College of Canada, PO Box 17000, Station Forces, Kingston, ON K7K 0C6, Canada

<sup>3</sup> Department of Physics and Space Sciences, Florida Institute of Technology, 150 W. University Blvd, Melbourne, FL 32904, USA

<sup>4</sup> Department of Physics, Engineering Physics and Astronomy, Queen's University, 99 University Avenue, Kingston, ON K7L 3N6, Canada

<sup>5</sup> Astrophysics group, Keele University, Keele, Staffordshire ST5 5BG, UK

<sup>6</sup> Kavli IPMU (WPI), Tokyo Institutes for Advanced Study, The University of Tokyo, 5-1-5 Kashiwanoha, Chiba 277-8583, Japan

Received 5 January 2017 / Accepted 7 February 2017

## ABSTRACT

Near-solar metallicity (and low-redshift) pair-instability supernova (PISN) candidates challenge stellar evolution models. Indeed, at such a metallicity, even an initially very massive star generally loses so much mass by stellar winds that it will avoid the electron-positron pair-creation instability. We use recent results showing that a magnetic field at the surface of a massive star can significantly reduce its effective mass-loss rate to compute magnetic models of very massive stars (VMSs) at solar metallicity and explore the possibility that such stars end as PISNe. We implement the quenching of the mass loss produced by a surface dipolar magnetic field into the Geneva stellar evolution code and compute new stellar models with an initial mass of  $200 M_{\odot}$  at solar metallicity, with and without rotation. This considerably reduces the total amount of mass lost by the star during its life. For the non-rotating model, the total (CO-core) mass of the models is  $72.8 M_{\odot}$  ( $70.1 M_{\odot}$ ) at the onset of the electron-positron pair-creation instability. For the rotating model, we obtain  $65.6 M_{\odot}$  ( $62.4 M_{\odot}$ ). In both cases, a significant fraction of the internal mass lies in the region where pair instability occurs in the  $\log(T) - \log(\rho)$  plane. The interaction of the reduced mass loss with the magnetic field efficiently brakes the surface of the rotating model, producing a strong shear and hence a very efficient mixing that makes the star evolve nearly homogeneously. The core characteristics of our models indicate that solar metallicity models of magnetic VMSs may evolve to PISNe (and pulsation PISNe).

**Key words.** stars: evolution – stars: magnetic field – stars: massive – stars: mass-loss – supernovae: general

## 1. Introduction

The discovery of pair instability supernovae (PISNe) candidates<sup>1</sup> at various redshifts in the past decade (e.g. Cooke et al. 2012, and including relatively low-redshift candidates, thus with a relatively high metallicity; Gal-Yam et al. 2009) has triggered great interest in understanding their formative pathways and initial attempts to model the evolution of the progenitors of such explosions. For a PISN explosion to occur, a significant fraction of the stellar mass must be located in the range of temperatures and densities where the pair-production instability occurs, leading to an adiabatic exponent  $\Gamma_{1, \text{ad}} < 4/3$ , which has a destabilising effect<sup>2</sup> (see e.g. Maeder 2009). This situation is reached for models with a CO-core mass in the range of about 60 to  $130 M_{\odot}$  (Heger & Woosley 2002; Chatzopoulos & Wheeler 2012).

Some superluminous supernovae (SLSNe) have been observed at solar and even higher metallicities (Lunnan et al. 2014). These supernovae might be associated to PISNe. With the high mass-loss rates typical of hot massive stars at solar metallicity, it is very unlikely for a very massive star (VMS) to match the

required end-of-life conditions to produce a PISN (Yusof et al. 2013). As a consequence, the existence of PISNe at such a metallicity would be a challenge for our understanding of the evolution of VMSs.

However, about 7% of Galactic O-type stars exhibit a measurable surface magnetic field (Wade et al. 2014)<sup>3</sup>. It has been shown that a surface dipolar magnetic field of sufficient strength (typically greater than about 1 kG) can considerably affect the winds from a hot massive star by confining part of the wind and preventing it from escaping the star (ud-Doula et al. 2008; Bard & Townsend 2016; Petit et al. 2017). Petit et al. (2017) explore the effects of the quenching of the wind by a surface magnetic field for stellar models between 40 and  $80 M_{\odot}$  at solar metallicity, and they show that the total mass lost during the main sequence (MS) can be considerably decreased compared to non-magnetic models.

In this paper, we apply the same procedure in the framework of VMSs at solar metallicity to assess the possibility of obtaining suitable PISN progenitors at higher metallicity than is usually thought. In Sect. 2 we summarise the physical modelling and parameters used for the stellar evolution computations. In

<sup>1</sup> Alternative explanations for these objects exist, see e.g. Moriya et al. (2010).

<sup>2</sup>  $\Gamma_{1, \text{ad}}$  is defined as  $\Gamma_{1, \text{ad}} = \left. \frac{\partial(\ln P)}{\partial(\ln \rho)} \right|_{\text{ad}}$ .

<sup>3</sup> This means a surface magnetic field stronger than about 100 G.

Sect. 3 we discuss the impact of the inclusion of the mass-loss quenching by magnetic field on the evolution of solar metallicity VMSs and compare our results with previous works. Finally, we present our conclusions in Sect. 4.

## 2. Physical modelling and parameters

We use the Geneva Stellar Evolution Code (Eggenberger et al. 2008) to perform the simulations of the current work in the same configuration as in Ekström et al. (2012). We refer to this work for the details of the various implementations used. Two important points have to be emphasised here:

- Our equation of state consists of a mixture of an ideal gas and radiation and accounts for the effects of partial ionisation. It does not include the effect of creation of electron-positron pairs, which would be necessary to perform an accurate simulation of the collapse towards a PISN (e.g. Chatzopoulos et al. 2015). However, our equation of state is suitable for providing the CO core mass and for estimating the fraction of the internal mass where pair creation occurs (see the discussion of Yusof et al. 2013).
- We use the same scheme for the computation of the mass-loss rates as used by Ekström et al. (2012): as long as the model has a surface hydrogen mass fraction  $X_S > 0.3$ , we use the Vink et al. (2000, 2001) rates. When the model enters the Wolf-Rayet star (WR) regime, that is, when  $X_S \leq 0.3$  with  $\log(T_{\text{eff}}) > 4.0$ , we use either the Gräfener & Hamann (2008) prescription in its validity domain, or the Nugis & Lamers (2000) prescription elsewhere. We note that when the Vink et al. (2000, 2001) mass-loss rates are higher than the Gräfener & Hamann (2008) or Nugis & Lamers (2000) rates, the Vink et al. (2000, 2001) prescription is used.

We implemented mass-loss quenching by the fossil surface magnetic field in the same way as Petit et al. (2017), by following the time evolution of a fossil surface dipolar field<sup>4</sup> (by assuming flux conservation). The escaping wind fraction  $f_B$  is given by

$$f_B = \frac{\dot{M}}{\dot{M}_{B=0}} = 1 - \sqrt{1 - \frac{r_\star}{r_c}}, \quad (1)$$

where  $r_c$  is the radius of the farthest closed loop of the magnetic field and is computed as a function of the Alfvén radius and the confinement parameter, and  $r_\star$  is the stellar radius (for details, see Petit et al. 2017; ud-Doula & Owocki 2002).

As stated by Petit et al. (2017), in the case of a rotating star,  $r_c$  should be replaced by the Keplerian co-rotation radius  $r_K$  if it is smaller than  $r_c$ . In practice, this never occurred in our simulations. For the computation of our rotating models, we assumed that the surface magnetic field of the star produces a braking of the surface. We imposed a torque as a boundary condition for the transport of angular momentum (ud-Doula et al. 2008), as in Meynet et al. (2011):

$$\frac{dJ}{dt} \approx \frac{2}{3} \dot{M}_{B=0} \Omega_\star^2 \left(0.3 + (\eta_\star + 0.25)^{\frac{1}{4}}\right)^2. \quad (2)$$

For the purpose of this paper, we computed two models of  $200 M_\odot$  at solar metallicity ( $Z_\odot = 0.014$ ), with an initial surface equatorial magnetic field  $B_{\text{eq}, \text{ZAMS}} = 1000$  G. We assume in

this work that the surface magnetic field evolves by conserving the magnetic flux throughout the whole evolution. One model is computed without rotation, and the other one with an initial equatorial velocity  $V_{\text{ini}}/V_{\text{crit}} = 0.4$ , where the critical velocity  $V_{\text{crit}} = \sqrt{\frac{2GM}{3R_{\text{p,b}}}}$ , with  $R_{\text{p,b}}$  being the polar radius at the break-up velocity (Maeder & Meynet 2000). Both models are evolved up to central oxygen burning.

## 3. Results

In this section, we discuss the most important results of our computations. We refer to our new models as “magnetic models”. We compare our models with the following models from Yusof et al. (2013): the  $200 M_\odot$  at solar metallicity, and the  $200 M_\odot$  at a lower metallicity ( $Z = 0.002$ ), corresponding to the metallicity of the Small Magellanic Cloud (SMC). We chose these models because 1) they were computed with the same stellar evolution code, which means that the differences are only due to the inclusion of mass-loss quenching and surface braking due to magnetic field (see previous section); 2) the lower metallicity model has lower mass-loss rates than the solar metallicity model, which makes it an interesting point of comparison with our new magnetic models; and 3) the SMC metallicity model retains enough mass ( $129.2 M_\odot$ ) to end as a PISN, whereas the rotating solar metallicity model with no magnetic quenching loses too much mass to end as a PISN (or even as a pulsation pair instability SN, PPISN, with a final mass of  $21.9 M_\odot$ , see Woosley 2016).

### 3.1. Mass loss and escaping wind fraction

The left panel of Fig. 1 shows the variation in total mass (top) and in the escaping wind fraction  $f_B$  defined in Eq. (1) for the magnetic models (thick lines, rotating model in black and non-rotating model in red), and for the solar-metallicity (black thin dashed line) and SMC-metallicity model (blue thin dashed line) from Yusof et al. (2013). During the MS,  $\eta_\star$  decreases because the stellar parameters evolve, causing the escaping wind fraction to grow from a value around 0.5 on the ZAMS to 0.8 near the end of the MS. For the non-rotating model, the oscillations between about 1.5 and 2 Myr are due to successive crossings of the bi-stability limit (Pauldrach & Puls 1990; Vink et al. 2000, 2001). The mass-loss rate on the cool side is considerably higher than on the hot side, therefore the escaping wind fraction is higher on the cool side. The change in the mass-loss rate keeps the star at the bi-stability limit for a while, generating the oscillations. After the MS, both models become very hot and compact WR stars (see the iso-radii in the right panel of Fig. 1 and Sect. 3.2), with a very low escaping wind fraction.

Magnetic wind quenching considerably reduces the total amount of mass lost during the evolution. Both magnetised models have a total mass of around  $70 M_\odot$  at the onset of central oxygen burning, while the corresponding non-magnetised model ends with about  $20 M_\odot$ . Overall, our solar metallicity models with magnetic fields show an evolution of the total mass in between the solar- and SMC-metallicity non-magnetic models (see also Fig. 2 of Petit et al. 2017).

### 3.2. Hertzsprung-Russell diagram tracks

The middle panel of Fig. 1 shows the tracks in the Hertzsprung-Russell diagram (HRD) of the four models (same colour code as left panel). The reduced mass-loss rates significantly change the tracks of the magnetic models compared to the corresponding

<sup>4</sup> Petit et al. (2017) took the magnetic field to be the (polar) dipolar field strength. In this paper,  $B_{\text{eq}}$  is to be understood as the equatorial magnetic field (ud-Doula et al. 2008; Meynet et al. 2011), the value of which is half of the dipolar field strength.

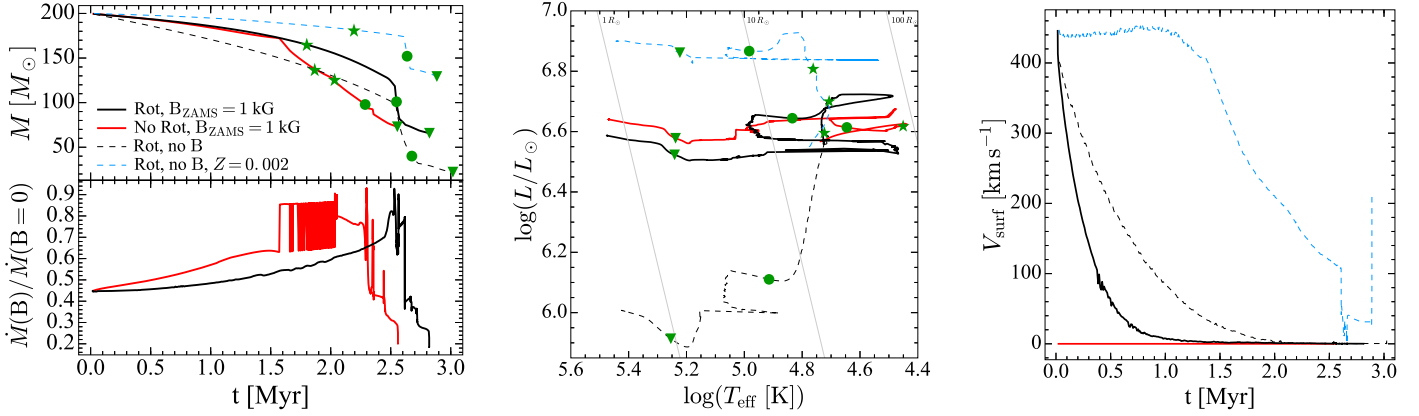


**Fig. 1.** *Left panel, top:* time evolution of the total mass of the models. The magnetic models computed for this work are plotted in black (rotating model) and red (non-rotating model). Models from [Yusof et al. \(2013\)](#) are shown for comparison: non-magnetic rotating model at solar metallicity (thin dashed black line) and SMC metallicity (thin dashed blue line). Key evolutionary phases are indicated: beginning of the WR phase (star), end of the MS (circle), and end of central He burning (triangle). *Left panel, bottom:* time evolution of the escaping wind fraction  $f_B$  (see Eq. (1)) for the magnetic rotating (black) and non-rotating (red) models. *Centre panel:* HRD tracks for the same models as in left panel. The meaning of the colours and symbols is the same. Iso-radii are indicated in light grey (1, 10, and 100  $R_\odot$  from left to right). *Right panel:* time evolution of the surface velocity of our models. We use the same colour scheme as for the top left panel.

solar-metallicity non-magnetic model: instead of evolving with decreasing luminosity, the magnetic models experience an increase in luminosity during the MS, as is seen in lower mass or lower metallicity models. When the mass loss has uncovered the hydrogen-burning core, the star enters a WR phase and becomes very hot. We note that rotating models evolve in a quasi-chemically homogeneous way, hence the almost vertical tracks during the MS (see e.g. [Maeder 1987](#); [Yoon & Langer 2005](#)). The mass loss is larger than that of the non-magnetic SMC metallicity model, however, causing the tracks to remain in a more limited range of luminosity than the SMC model from [Yusof et al. \(2013\)](#).

### 3.3. Surface and internal velocities

The right panel of Fig. 1 shows the time evolution of the surface velocity of the models. Even with a considerably reduced mass loss compared to the non-magnetic case, the surface of the rotating magnetic model experiences a much stronger braking that is due to the coupling between the stellar wind and the magnetic field ([Meynet et al. 2011](#)). The surface velocity drops below  $100 \text{ km s}^{-1}$  in about 0.5 Myr. Thus, we expect VMSs with an external magnetic field to be slow rotators, even if their mass-loss rates are decreased with respect to the non-magnetic case.

When the magnetised models avoid exploding as PISNe (see Sect. 3.4), it is interesting to determine the amount of angular momentum retained in the core near the end of the evolution. As illustrated by the evolution of the surface velocities, the angular momentum lost by the magnetic models is higher than in the non-magnetic case, even though the mass-loss rate is reduced. This is due to the increased torque exerted on the surface because of the magnetic field (see Eq. (2)). The extraction of angular momentum from the core is efficient enough to prevent the formation of a long-soft gamma-ray burst through the collapsar scenario (see also the discussion of [Yusof et al. 2013](#)).

### 3.4. Central conditions and possible PISN progenitor

The evolution of the central temperature as a function of the central density is shown in the left panel of Fig. 2. As expected from the time evolution of the total mass (top left panel of Fig. 1), both

non-rotating and rotating magnetic models evolve in between the solar-metallicity and SMC-metallicity model from [Yusof et al. \(2013\)](#). In contrast to the SMC-metallicity model, which enters the temperature-density domain where electron-pair creation occurs (grey shaded area, from [Chatzopoulos et al. 2015](#)), both our magnetic models only graze this region. However, a significant fraction of the internal mass of these models crosses it (centre panel). This is illustrated by the thin black lines with blue (beginning of central oxygen burning) or red (end of central oxygen burning) dots, showing the temperature-density profile inside the magnetic rotating model. The dots are positioned at every 10% of the internal mass. At the beginning of the central oxygen burning, about 30% of the internal mass is in the region with  $\Gamma_{1, \text{ad}} < 4/3$ . This fraction reaches about 50% at the end of central oxygen burning. The right panel of Fig. 2 shows the internal density profile as a function of the mass coordinate. The thick parts of the curves indicate the region inside the star lying inside the pair-creation region at the beginning (blue) and end (red) of central oxygen burning, illustrating the contraction of the model during this phase, as well as the growth of the region inside the pair-creation region with time.

Moreover, the mass of the CO core of our magnetic models is  $70.1 M_\odot$  (non-rotating model) and  $62.4 M_\odot$  (rotating model). This is in the range of mass leading to PISN explosion according to [Heger & Woosley \(2002\)](#). With the large portion of the internal mass inside the region with  $\Gamma_{1, \text{ad}} < 4/3$ , it is thus plausible (see [Fowler & Hoyle 1964](#)) that VMS models with magnetic quenching of the stellar winds lead to PISN progenitors at a higher metallicity than usually considered when a standard mass loss is applied. Models with the same initial mass but a slightly higher initial magnetic field or models with a slightly higher initial mass will also penetrate the  $\Gamma_{1, \text{ad}} < 4/3$  region more deeply.

We also emphasise that our choice of initial magnetic field strength is modest and hence the mass-loss quenching we obtain is small compared to what it would be with a higher initial field. Moreover, our models always evolve at a high enough effective temperature to never have a large external convective zone that would probably destroy the fossil magnetic field hypothesised in this work. Another point is that because of the strong mass-loss, layers that were previously located inside the convective core, where a dynamo could be active, are uncovered

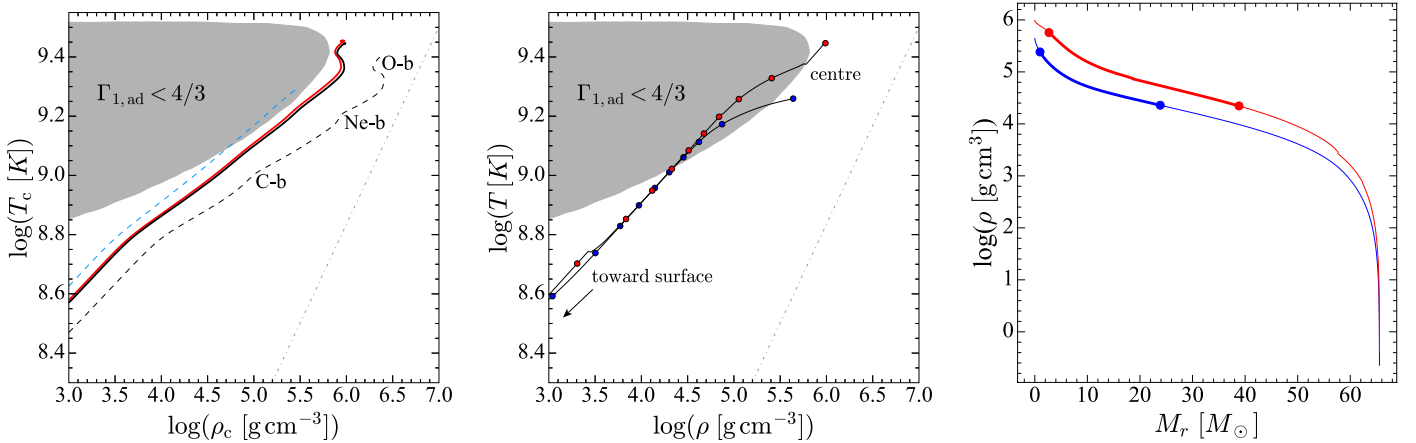


**Fig. 2.** *Left panel:* evolutionary tracks in the central temperature versus central density diagram. The colours of the tracks have the same meaning as in the top left panel of Fig. 1. The thin grey dot-dashed line represents the transition between the perfect gas and degenerate gas domains. The shaded grey zone shows the region of the diagram where electron-pair creation occurs and is adopted from Chatzopoulos et al. (2015). *Centre panel:* internal profiles of the magnetic rotating model at the beginning (blue dots) and end (red dots) of central oxygen burning. The dots are spaced by 10% of the total mass of the star. *Right panel:* internal density profiles (as a function of the mass coordinate) at the beginning (blue) and end (red) of central oxygen burning. The thick part of the curves indicates the region inside the star inside the electron-pair creation region.

relatively quickly. The effect on the global dipolar field is unknown, and studying it is beyond the scope of this paper. If our assumption of flux conservation breaks down at some point in the evolution, then the total mass lost by our models would be higher and hence disfavour our scenario for a high-metallicity PISN progenitor. Additional mass loss may occur as the Eddington factor reaches high values towards the end of the evolution (see Fig. 9 in Yusof et al. 2013, and the corresponding discussion). In any case, magnetic quenching is more favourable to VMSs at high(er) metallicities undergoing the pulsation pair-instability (see Woosley 2016, and references therein).

Our modelling considers steady-state mass loss. As our models evolve close to the Eddington limit ( $L/L_{\text{Edd}} = 0.5\text{--}0.7$  during the MS, but up to 0.9 at the very end of the evolution), it is possible that eruptive mass-loss events may occur. However, such events are currently unpredictable and are not modelled in stellar evolution codes. It is therefore difficult to quantify the effect they may have on the scenario discussed here.

## 4. Conclusions

Observations show that about 7% of O-type stars have a strong fossil surface dipolar magnetic field at solar metallicity, ranging from a few 100 G to about 20 kG (Wade et al. 2014). It has been shown that such surface magnetic fields are able to significantly quench the mass loss from the star (Petit et al. 2017).

In this paper, we explored the effect of such a mass-loss quenching on the evolution of VMSs at solar metallicity in case of a modest surface magnetic field of 1000 G. We showed that this mechanism is able to reduce the total mass lost during the evolution in such a way that the models end with a massive CO core and with a significant fraction of their internal mass in the density and temperature domain where electron-pair creation is possible. This mechanism therefore leads to a plausible scenario to form PISN at higher metallicity than is usually thought, and it could help in explaining SLSNe in the local Universe. The rarity of VMSs at near-solar metallicity (Martins 2015) and the small fraction of massive stars exhibiting fossil surface magnetic fields provides a natural explanation of the scarcity of such events at high metallicity (Lunnan et al. 2014).

In the future, we intend to explore the parameter space of the initial mass  $M_{\text{ZAMS}}$  and initial magnetic field strength  $B_{\text{ZAMS}}$

more extensively to determine the initial parameters leading to PISNe (and pulsation-PISNe). A complete study of the possibility of PISN explosion and of the lightcurve expected is also planned, as was done for models from Yusof et al. (2013) in Kozyreva et al. (2017).

*Acknowledgements.* C.G., G.M., and S.E. acknowledge support from the Swiss National Science Foundation (project number 200020-160119). G.A.W. acknowledges Discovery Grant support from the Natural Sciences and Engineering Research Council (NSERC) of Canada. V.P. acknowledges support provided by the NASA through *Chandra* Award Number GO3-14017A issued by the *Chandra* X-ray Observatory Center, which is operated by the Smithsonian Astrophysical Observatory for and on behalf of the NASA under contract NAS8-03060. R.H. acknowledges support from EU-FP7-ERC-2012-St Grant 306901 and from the World Premier International Research Center Initiative (WPI Initiative, MEXT, Japan).

## References

- Bard, C., & Townsend, R. H. D. 2016, *MNRAS*, 462, 3672  
Chatzopoulos, E., & Wheeler, J. C. 2012, *ApJ*, 748, 42  
Chatzopoulos, E., van Rossum, D. R., Craig, W. J., et al. 2015, *ApJ*, 799, 18  
Cooke, J., Sullivan, M., Gal-Yam, A., et al. 2012, *Nature*, 491, 228  
Eggenberger, P., Meynet, G., Maeder, A., et al. 2008, *Ap&SS*, 316, 43  
Ekström, S., Georgy, C., Eggenberger, P., et al. 2012, *A&A*, 537, A146  
Fowler, W. A., & Hoyle, F. 1964, *ApJS*, 9, 201  
Gal-Yam, A., Mazzali, P., Ofek, E. O., et al. 2009, *Nature*, 462, 624  
Gräfener, G., & Hamann, W.-R. 2008, *A&A*, 482, 945  
Heger, A., & Woosley, S. E. 2002, *ApJ*, 567, 532  
Kozyreva, A., Gilmer, M., Hirschi, R., et al. 2017, *MNRAS*, 464, 2854  
Lunnan, R., Chornock, R., Berger, E., et al. 2014, *ApJ*, 787, 138  
Maeder, A. 1987, *A&A*, 178, 159  
Maeder, A. 2009, *Physics, Formation and Evolution of Rotating Stars* (Springer)  
Maeder, A., & Meynet, G. 2000, *A&A*, 361, 159  
Martins, F. 2015, in *Very Massive Stars in the Local Universe*, ed. J. S. Vink, *Astrophys. Space Sci. Lib.*, 412, 9  
Meynet, G., Eggenberger, P., & Maeder, A. 2011, *A&A*, 525, L11  
Moriya, T., Tominaga, N., Tanaka, M., Maeda, K., & Nomoto, K. 2010, *ApJ*, 717, L83  
Nugis, T., & Lamers, H. J. G. L. M. 2000, *A&A*, 360, 227  
Pauldrach, A. W. A., & Puls, J. 1990, *A&A*, 237, 409  
Petit, V., Keszthelyi, Z., MacInnis, R., et al. 2017, *MNRAS*, 466, 1052  
ud-Doula, A., & Owocki, S. P. 2002, *ApJ*, 576, 413  
ud-Doula, A., Owocki, S. P., & Townsend, R. H. D. 2008, *MNRAS*, 385, 97  
Vink, J. S., de Koter, A., & Lamers, H. J. G. L. M. 2000, *A&A*, 362, 295  
Vink, J. S., de Koter, A., & Lamers, H. J. G. L. M. 2001, *A&A*, 369, 574  
Wade, G. A., Grunhut, J., Alecian, E., et al. 2014, in *IAU Symp.*, 302, 265  
Woosley, S. E. 2016, *ApJ*, submitted [[arXiv:1608.08939](https://arxiv.org/abs/1608.08939)]  
Yoon, S.-C., & Langer, N. 2005, *A&A*, 443, 643  
Yusof, N., Hirschi, R., Meynet, G., et al. 2013, *MNRAS*, 433, 1114